

Linköping Studies in Science and Technology  
Licentiate Thesis No. 1552

PHYSICAL VAPOR DEPOSITION OF YTTRIA-STABILIZED  
ZIRCONIA AND GADOLINIA-DOPED CERIA THIN FILMS  
FOR FUEL CELL APPLICATIONS

Steffen Sønderby



**Linköping University**  
**INSTITUTE OF TECHNOLOGY**

LIU-TEK-LIC-2012:37  
Thin Film Physics Division  
Department of Physics, Chemistry and Biology (IFM)  
Linköping University  
SE-581 83 Linköping, Sweden

© Steffen Sønderby, 2012  
ISBN 978-91-7519-767-8  
ISSN: 0280-7971  
Printed by LiU-Tryck  
Linköping, Sweden, 2012

# ABSTRACT

---

In this thesis, reactive sputter deposition of yttria-stabilized zirconia (YSZ) and cerium gadolinium oxide (CGO) thin films for solid oxide fuel cell (SOFC) applications have been studied. All films have been deposited under industrial conditions.

YSZ films were deposited on silicon wafers as well as commercial NiO-YSZ fuel cell anodes. The texture, morphology, and composition of the deposited films were investigated with respect to deposition parameters such as bias voltage which was identified as a key parameter to tailor the texture of the film and promote less columnar coatings when depositing on Si. In contrast, films grown on NiO-YSZ fuel cell anodes were seen to be randomly orientated when deposited at low substrate bias voltages. When the bias voltage was increased the film took over the orientation of underlying substrate due to substrate template effects. The deposited coatings were found to be homogeneous large areas within the coating zone, which is highly important for industrial applications.

The performance of sputtered CGO thin films as diffusion barriers for stopping Sr diffusion between SOFC cathodes and electrolytes was also studied. This was done by introducing the sputtered CGO films in a metal-based SOFC setup. The performance depended on the density of the barrier layer, signifying that Sr diffusion and SrZrO<sub>3</sub> formation is an issue. Area specific resistances down to 0.27 Ωcm<sup>2</sup>, corresponding to a maximum power density up to 1.14 W cm<sup>-2</sup> at 650 °C could be obtained with sputtered CGO barrier layers in combination with Sr-doped lanthanum cobalt oxide cathodes which is a significant improvement compared conventional ceramic SOFCs.

The diffusion mechanism of Sr through sputtered CGO films was investigated. For this purpose, a model system simulating a SOFC was prepared by depositing CGO and YSZ on cathode material. This setup allowed observation of Sr diffusion by observing SrZrO<sub>3</sub> formation using X-ray diffraction while annealing. Electron microscopy was subsequently performed to confirm the results. It was found that Sr diffused along column/grain boundaries in the CGO films but by modifying the film thickness and microstructure the breaking temperature of the barrier could be increased.



## PREFACE

---

This Licentiate Thesis is part of my PhD studies in the Thin Film Division at Linköping University and the Tribology Centre at the Danish Technological Institute. The aim of my research is to develop thin film electrolytes and diffusion barrier coatings for solid oxide fuel cells in order to increase the performance and decrease the operation temperature of the fuel cells and thereby bring this technology out of the laboratory and closer to practical application. The research is directly financially supported by Topsøe Fuel Cell and Nordforsk under the Private Public Partnership (PPP) PhD program (contract no. 9046). The purposes of the PPP PhD Program are to increase knowledge exchange between the Nordic countries and promote collaboration between industry and academia. Funding from this scheme requires the PhD student to be employed at a company in one Nordic country while studying in another Nordic country. In my case, this means being employed at the Danish Technological Institute, Denmark, while studying at Linköping University, Sweden where I spend 2/3 and 1/3 of my time, respectively.

Additional financial support has been given by Nordic Innovation Centre (contract no. 09046), and the Swedish Foundation for Strategic Research (Ingvar Carlsson Award 3 to my supervisor Per Eklund).



## INCLUDED PAPERS

---

### Paper 1

#### **Reactive magnetron sputtering of uniform yttria-stabilized zirconia coatings in an industrial setup**

**S. Sønderby**, A. J. Nielsen, B. H. Christensen, K. P. Almqvist, J. Lu, J. Jensen, L. P. Nielsen, and P. Eklund

*Surface & Coatings Technology*, **206** (2012) 4126.

### Paper 2

#### **High performance metal-supported solid oxide fuel cells with Gd-doped ceria barrier layers**

T. Klemensø, J. Nielsen, P. Blennow, Å. H. Persson, T. Stegk, B. H. Christensen, and **S. Sønderby**

*Journal of Power Sources*, **196** (2011) 9459.

### Paper 3

#### **Strontium diffusion in magnetron sputtered gadolinia-doped ceria thin film barrier coatings for solid oxide fuel cells**

**S. Sønderby**, P. Lunca Popa, J. Lu, B. H. Christensen, K. P. Almqvist, L. P. Nielsen, and P. Eklund

*Manuscript submitted for publication.*

**My contribution to the included papers:**

**Paper 1:**

I was involved in the planning, performed a large part of the characterization and analysis, and wrote the paper.

**Paper 2:**

I was involved in the planning, performed all sputter depositions and part of the characterization.

**Paper 3:**

I was responsible for the planning and analysis, performed all synthesis and most characterization, and wrote the paper.

## PUBLICATIONS NOT INCLUDED IN THE THESIS

---

### Paper 4

#### **Optimization of the mechanical properties of magnetron sputtered diamond-like carbon coatings**

S. Sønnerby, A. N. Berthelsen, K. P. Almtoft, B. H. Christensen, L. P. Nielsen, and J. Bøttiger

*Diamond and Related Materials*, **20** (2011) 682.

### Paper 5

#### **Development of Long-Term Stable and High-Performing Metal-Supported SOFCs**

T. Klemensø, J. Nielsen, P. Blennow, A. Persson, T. Stegk, P. Hjalmarsen, B. Christensen, S. Sønnerby, J. Hjelm, and S. Ramousse

*ECS Transactions*, **35** (2011) 369.



## ACKNOWLEDGMENTS

---

I am grateful to a large number of people who have contributed, helped, and supported me during the course of my work. In particular I would like to thank:

- Per Eklund, my main supervisor.
- Colleagues at the Tribology Center at the Danish Technological Institute in Aarhus.
- Colleagues at IFM, in particular those in the Thin Film Physics, Plasma & Coatings Physics, and Nanostructured Materials groups.
- Co-authors of the papers.
- Collaborators at Risø.
- Collaborators at the Materials Science Group at Aarhus University.
- Collaborators at Topsøe Fuel Cell.
- My family and friends.



# TABLE OF CONTENT

---

Abstract .....	i
Preface .....	iii
Included Papers .....	v
Publications not included in the thesis.....	vii
Acknowledgments.....	ix
1. Introduction .....	1
1.1 Thin films .....	1
1.2 Fuel cells .....	1
1.3 Objective.....	2
2. Solid oxide fuel cells .....	5
2.1 Principle of operation .....	5
2.2 Cell and stack design.....	7
2.3 Anode materials.....	7
2.4 Cathode materials.....	8
2.5 Electrolyte materials.....	9
2.6 Interconnects .....	9
2.7 Sealing .....	10
2.8 Structural support of the cell .....	10
3. Film deposition.....	13
3.1 Sputter deposition.....	13
3.2 DC glow discharge.....	14
3.3 The sputtering phenomenon .....	16
3.4 Effects on the substrate .....	16
3.5 DC magnetron sputtering.....	17
3.6 Reactive sputtering .....	18
3.7 Pulsed DC magnetron sputtering .....	19
3.8 Setup .....	19
4. Characterization techniques.....	21
4.1 X-ray Diffraction (XRD) .....	21
4.2 Scanning Electron Microscopy (SEM).....	22
4.3 Transmission Electron Microscopy (TEM).....	23
4.4 Energy Dispersive X-ray Spectroscopy (EDX or EDS).....	24

4.5	Ion-beam analysis.....	25
5.	Cell testing.....	27
5.1	Polarization curves .....	27
5.2	Electrochemical Impedance spectroscopy (EIS) .....	28
6.	Summary of the appended papers.....	31
7.1	Deposition of YSZ.....	31
7.2	Deposition of CGO.....	32
7.	Current activities and Future plans.....	35
8.	References .....	37

# 1. INTRODUCTION

---

## 1.1 Thin films

Since the 1950s, the coating industry has expanded rapidly and today thin films are found in numerous applications. By applying a coating with thickness ranging from a few nanometers to several micrometers, a surface with properties significantly different from those of the bulk material can be obtained. This allows the bulk material to be chosen based on requirements for mechanical support, stability, and cost. By surface treatment, the appropriate thin film can be applied to achieve unique or improved properties. For instance, coatings with improved wear or corrosion resistance, improved electrical or optical properties, or simply decorative purposes can be applied [1].

Among the many different techniques for thin film deposition, sputtering is one of the oldest. The sputtering phenomenon was observed by William R. Grove in the mid-1800s [2]. Since then, the technique has advanced considerably and is still being improved today. The constant development of the sputtering technology is driven by increasing commercial demands and a desire to offer improved coating for new applications.

## 1.2 Fuel cells

Despite the current economic crisis, the demand for energy has been continuously growing and is expected to continue growing for the coming decades due to increasing world population and economic development, especially in Asia [3]. Therefore, the development of new power generation technologies has become increasingly relevant. In that perspective, solid oxide fuel cells (SOFC) is a technology subject to intense research as SOFCs have the potential to convert chemical energy to electrical energy with high efficiency and thereby significantly reduce CO<sub>2</sub> emissions [4]. In addition, fuel cells are modular in design which enables decentralization of the power grid by installation of small units for domestic energy supply and thereby improved security of supply. Furthermore, a fuel cell can also be operated in the reverse mode, as an electrolysis cell, to split water into hydrogen and oxygen using

electricity from e.g. a windmill [5]. In conclusion, fuel cell technology may become important in an energy system based on renewable energy.

The fuel cell concept has been known since the 19<sup>th</sup> century when it was invented by Grove [6] who also described the sputtering phenomenon. Since then, different types of fuel cells were developed. Today, the five main types of fuel cells are the alkaline fuel cell (AFC), the phosphoric acid fuel cell (PAFC), the molten carbonate fuel cell (MCFC), the polymer electrolyte membrane fuel cell (PEMFC), and the solid oxide fuel cell (SOFC). They all consist of an anode, a cathode, and an electrolyte which separates the two electrodes. Fuel cells are classified by and named after the chemical characteristics of the electrolyte but the general principle of operation is the same for all cells. The type of electrolyte dictates the operation temperature and other performance characteristics which makes different types of cells suitable for certain applications [4,7].

Earlier on research focused mostly on fuel cells working at low temperature such as PEMFC and AFC which were used in the space program in the 1960s [8], whereas today SOFC technology is in focus as it is expected to have large market potential when it fully matures. Before commercialization of the SOFC technology, issues regarding scale-up, increasing lifetime of the components, and reducing the system price needs to be addressed.

Deposition of thin films by different physical vapor deposition (PVD) techniques is being studied as a potential way to address these issues. For instance, the use of thin film electrolytes with thicknesses down to a few micrometers can minimize ohmic losses related to the electrolyte, and reduce the operation temperature of the SOFC to an intermediate domain of 500–700 °C, which will increase cell lifetime and reduce the costs of components. Previous investigations have demonstrated laboratory scale deposition of thin films for SOFCs by techniques such as pulsed laser deposition (PLD) [9], atomic layer deposition (ALD) [10], electron beam physical vapor evaporation (EB-PVD) [11], and magnetron sputtering [12-15].

### 1.3 Objective

The objective of this work is to contribute towards the commercialization of the SOFC technology. For this purpose two tracks are pursued. Firstly, thin film SOFC electrolytes deposited by reactive magnetron sputtering are explored. This includes both growth and characterization of yttria-stabilized zirconia (YSZ), with the goal of producing a thin, uniform

and dense coating, and subsequent performance testing of SOFCs with sputtered YSZ electrolytes. The second track focuses on deposition and characterization of cerium gadolinium oxide (CGO) thin film diffusion barriers, placed between the SOFC cathode and electrolyte. This is of interest as novel, high performing Fe-Co perovskite-based cathode materials contain Sr which will react with the SOFC YSZ electrolyte unless a barrier material, such as CGO, is applied. This path involves both deposition and characterization of CGO thin films, performance testing of SOFCs with CGO barriers, and studies of the diffusion mechanism of strontium in sputtered CGO. In order to demonstrate the feasibility of large-scale deposition of thin films for SOFC application, depositions are carried out using an industrial batch coating system.



## 2. SOLID OXIDE FUEL CELLS

---

In this section, a short introduction to the SOFC is given. This includes the principle of operation, considerations for cell design, and materials used to produce SOFCs.

### 2.1 Principle of operation

The fuel cell works by converting chemically bound energy directly into electricity and heat. The basic building blocks of the fuel cell are an electrolyte sandwiched between a porous anode and cathode. On the anode side fuel is continuously fed and oxidized, while on the cathode side oxygen is reduced. Oxygen ions are transported through the electrolyte and electrons pass through an external circuit producing an electric current. The operation of the SOFC is sketched in figure 2.1. The cell potential difference generated between the electrodes by the cell reactions ( $\Delta U_{cell}$ ) is defined by the electromotive force ( $EMF$ ), the potential drop associated with operation of the cell ( $\Delta U_{current}$ ), and voltage losses due to leaks in the cell ( $\Delta U_{leak}$ ) as

$$\Delta U_{cell} = EMF - \Delta U_{current} - \Delta U_{leak} \quad (2.1)$$

The  $EMF$  is the theoretical potential difference when the current density is zero and is determined by the Nernst equation

$$EMF = \Delta U_{cell}^0 - \frac{R \cdot T}{z \cdot F} \cdot \ln Q \quad (2.2)$$

where  $\Delta U_{cell}^0$  is potential under standard conditions (25 °C, 1 atm),  $R$  is the gas constant,  $T$  the temperature,  $z$  the number of electrons involved,  $F$  is Faraday's constant, and  $Q$  the reaction quotient. The potential drop associated with operation of the cell is related to the current density and result from ohmic resistance ( $R_{ohmic}$ ) in the cell components and from polarization resistance ( $\eta$ ) due to limitations on the reaction rates. It can be written as

$$\Delta_{current} = i \cdot R_{ohmic} + \eta(i) \quad (2.3)$$

As it can be seen from the above formulas, the cell potential depends on the type and composition of the supplied fuel, the cell materials, the operation temperature, and current density. The work presented in this thesis focuses on reducing the ohmic resistance of the electrolyte and the electrolyte-cathode interface in order to operate the cell at lower temperatures without loss of performance. A more thorough description of the thermodynamic principles and operation of fuel cells can be found in several textbooks and handbooks [16,17].

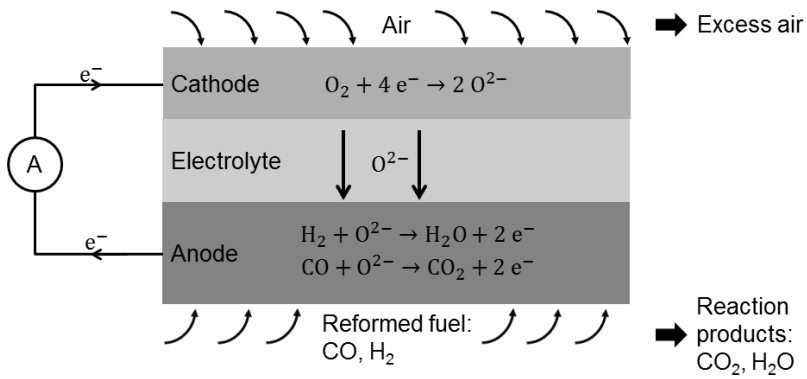


Figure 2.1: Schematic diagram showing the principle of a solid oxide fuel cell.

The SOFC uses a solid ceramic oxide as an electrolyte and requires operation at elevated temperatures, typically between 700 – 1000 °C, in order to facilitate the transport of oxide ions through this electrolyte. The SOFC is characterized by high conversion efficiencies of up to 70 % [7] and the ability to run directly on hydrocarbon fuel as the high operation temperature facilitates internal reforming of hydrocarbons to CO and H<sub>2</sub>. These features, and the fact that it takes time to reach the operation temperature, make SOFCs best suitable for applications such as stationary power plants where the excess heat generated in the process can be recovered. Another example is auxiliary power units (APUs) for trucks to produce electricity more efficiently than idling the engine which is environmentally detrimental.

## 2.2 Cell and stack design

A typical SOFC operates at a potential  $< 1$  V and delivers typically  $0.5\text{-}1.5$  W/cm<sup>2</sup>, however, this number is highly temperature dependent [18-20]. For most practical applications, SOFCs therefore need to be combined into a stack in order to obtain the required voltage and power output required for the application. This is done by connecting cells in series via electrically conducting interconnects. For stacking, there are two prevailing cell designs: the tubular and the planar cell. In the tubular design, the tube-shape gives the cell a high structural robustness and yields significant advantages in sealing [16]. The planar cells have a more simple geometry making them cheaper to manufacture, easier to stack together in a compact way, and gives the shortest current path [17,21]. This thesis deals with planar cells which also are well suited for PVD due to planar geometry. Figure 2.2 shows a schematic drawing of the planar stack design. All cell and stack components are described in detail in the following sections.

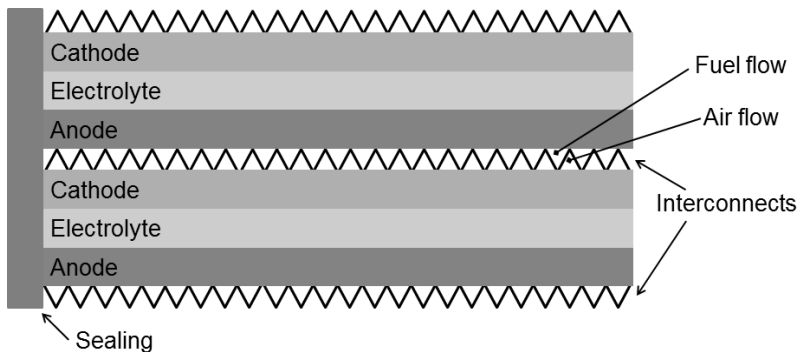


Figure 2.2: Schematic drawing of planar stack design.

## 2.3 Anode materials

The most common material for SOFC anodes is a porous Ni/YSZ cermet where YSZ provides oxide ion conductivity, while Ni serves to reform hydrocarbon fuel and facilitates the oxidation of the fuel. This reaction takes place in the three phase boundaries, where the YSZ and Ni grains meet the fuel gas phase. The anode requires a porosity of more than 30 vol.% to ensure transport of fuel to the reaction sites and the removal of reaction products [22] as well

as at least 30 vol.% Ni in order to be electrically conducting and function effectively as an electrode [4]. Anodes are typically prepared by sintering of a NiO/YSZ composite followed by a reduction when exposed to the fuel gases which result in the needed porosity. Dispersion of Ni in the YSZ prevents coarsening of Ni particles during operation, and also gives the anode a thermal expansion coefficient comparable to that of the electrolyte.

## 2.4 Cathode materials

The cathode is exposed to high temperature and an oxidizing atmosphere which limits the choice of materials to noble metals and conducting oxides. The most popular materials for SOFC cathodes belong to the family of perovskite-type oxides. It is possible to alter the physical and chemical properties of these materials by substituting metal ions. The cathode needs to have a high catalytic activity towards oxygen reduction, be able to conduct electrons as well as oxide ions, and have a porous microstructure to allow transport of oxygen [4,23]. The most commonly used cathode for zirconia-based SOFCs is a composite of YSZ and  $\text{La}_{1-x}\text{Sr}_x\text{MnO}_3$  (LSM). The YSZ phase in the composite provides the oxide ion conductivity while the LSM facilitates the catalytic activity and is electronic conductive. The reaction takes place in the triple phase boundary. LSM based cathodes are only satisfactorily efficient at elevated temperatures. At intermediate temperatures (around 750 °C) other perovskite-type oxides such as mixed ionic and electronic conductors  $\text{La}_{1-x}\text{Sr}_x\text{Co}_{1-y}\text{Fe}_y\text{O}_3$  (LSCF) and  $\text{La}_{1-x}\text{Sr}_x\text{CoO}_3$  (LSC) are superior to LSM-type cathodes due to lower area-specific resistance. However, these types of cathodes are incompatible with YSZ electrodes as Sr from the cathode reacts with Zr from the electrolyte during operation, which results in the formation of a layer of low conducting  $\text{SrZrO}_3$  that have a detrimental effect on the performance of the cell [23]. Therefore, a diffusion barrier layer is needed between the cathode and the electrolyte. In contrast to YSZ, CGO does not react with Sr from cathode materials such as LSC and LSCF. This property makes CGO suitable as a diffusion barrier layer placed between the LSCF cathode and the YSZ electrolyte [23-25]. The ability of CGO barriers to prevent Sr diffusion is depending on layer thickness and microstructure as well as operation temperature [26]. In *paper 3*, I study Sr diffusion through sputtered CGO barriers.

## 2.5 Electrolyte materials

It is required of the electrolyte that it be dense to separate fuel from oxygen, be electrically insulating, and an ionic conductor. The most widely used material is YSZ as it has a satisfactory ionic conductivity, show good stability in both reducing and oxidizing environments, and is abundant and relatively low in cost [27]. Pure zirconia ( $\text{ZrO}_2$ ) is monoclinic at room temperature, transforms to the tetragonal phase above 1170 °C, and to the cubic structure above 2370 °C. By substituting some  $\text{Zr}^{4+}$  ions with ions of lower valence, such as  $\text{Y}^{3+}$ , it is possible to stabilize the zirconia in the cubic fluorite structure from room temperature and up to the melting point. At the same time, oxygen vacancies are introduced to maintain charge neutrality and allow oxygen migration. The ionic conductivity is at a maximum near the minimum level of dopant required to stabilize the cubic phase. Therefore, YSZ typically contains 8-10 mol% yttria ( $\text{Y}_2\text{O}_3$ ) [4,28]. CGO has also been proposed as an electrolyte material as it has a high conductivity and therefore can be used at a lower temperature relative to YSZ. However, at temperatures about 600 °C a significant reduction of  $\text{Ce}^{4+}$  to  $\text{Ce}^{3+}$  can take place in the reducing atmosphere found on the fuel side. This reduction creates lattice stress and the CGO becomes a mixed conductor which significantly reduces its efficiency as electrolyte [29,30].

Research is being carried out to develop thin film electrolytes by PVD [19] or wet chemical techniques [31,32] in order to lower the ohmic resistance losses in the electrolyte and thereby lower the operation temperature of the SOFC [28,33].

## 2.6 Interconnects

When stacking SOFCs, interconnects connect cells in series electrically, and separate air at the cathode side of one cell from fuel on the at the anode side of a neighboring cell. Therefore, interconnects are required to be gas tight, have a high electronic conductivity, and stable in both reducing and oxidizing atmospheres. Traditionally, ceramic  $\text{LaCrO}_3$  interconnects have been applied for high temperature SOFCs. By reducing the operation temperature of the SOFC to 600 – 800 °C steel-based metallic interconnects can be used instead. Compared to ceramic interconnects these steel-based interconnect provide mechanical support, are easier to process, and cheaper [34].

## 2.7 Sealing

To prevent the oxidant from reaching the fuel so as to avoid mixing of the reactants with the ambient, sealing of the SOFC is needed. The sealing material needs to be electrically insulating, stable towards all other cell components as well as the atmospheric conditions. In order to obtain a tight seal a match between the thermal expansion coefficients of the seal and the cell components as well as a degree of deformability is essential. For SOFCs seals are typically glass-based [35].

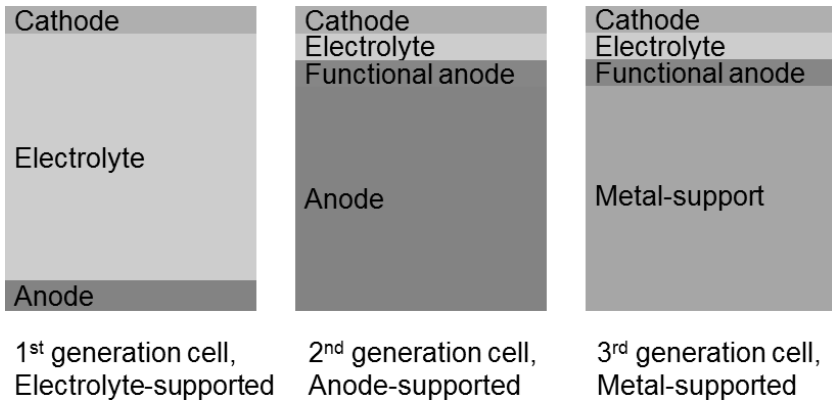


Figure 2.3: Sketch of the three generations of planar cells.

## 2.8 Structural support of the cell

Three designs for bringing structural support and mechanical strength to the planar cell have been developed. These designs are based on electrolyte-, anode-, and metal-support and are known as first, second, and third generation cells, respectively. A sketch showing the three designs are seen in figure 2.3. The first developed design was based on a hundreds of micrometer thick electrolyte to support the cell. As a consequence, operation temperatures around 1000 °C was needed to obtain reasonable performance. Other cell components, such as interconnects, capable of operating in this temperature range are complex and expensive which makes lower temperatures desirable. The second generation cell is based on anode-support. In this design, the anode is divided into a functional top layer and a thick supporting layer. This design allows for thin electrolytes and can operate at temperatures below 800 °C.

The third-generation design utilizes thin ceramic functional layers for the anode and a robust porous metal layer beneath the anode functional layer for mechanical support. Compared to cells based on ceramic support, this design provides substantial advantages with respect to materials and manufacturing costs as well as improved mechanical properties. For some applications, such as APUs, the improved robustness and tolerance to dynamic operation, including fast start-up, thermal cycling, and shock vibrations are important [29]. Due to the metal-support, third generation cells are intended to operate at temperatures below 800 °C in order to prevent corrosion of the metal.

In this work, YSZ electrolyte coatings of have been deposited on anode-supports (*paper 1*) and CGO barrier coatings have been deposited on electrolytes on metal-supported cells (*paper 2*). In *paper 3*, CGO and YSZ depositions have been carried out on LSCF cathodes.



## 3. FILM DEPOSITION

---

Several techniques exist for thin film synthesis. In this work, sputtering has been used. This section gives a short introduction to the sputtering technique and the physics of sputtering.

### 3.1 Sputter deposition

In a sputtering process, atoms are ejected from a target material due to bombardment by energetic particles. Figure 3.1 shows a simple schematic drawing of a sputtering system. Inside a vacuum chamber, two electrodes are placed. Typically, the chamber walls will act as anode whereas a target, made of the material to be deposited, is connected to the negative terminal of a power supply and serves as the cathode. The object to be coated (the substrate) is placed in front of the target. The substrate can be biased or at a floating potential. To form plasma, an inert working gas such as argon is introduced into the chamber.  $\text{Ar}^+$ -ions of the working gas are accelerated towards the target by the electric field between the electrodes. Upon impact, neutral atoms will be ejected from the target through momentum transfer from the energetic  $\text{Ar}^+$ -ions. The sputtered atoms pass through the discharge and condense onto the substrate to grow a film. Besides sputtering of neutral atoms the impacts also eject secondary electrons. These electrons collide with the neutral gas atoms and form more ions which return to the cathode. Thus, the plasma becomes self-sustaining when the number of ejected secondary electrons is sufficient to produce the required ions.

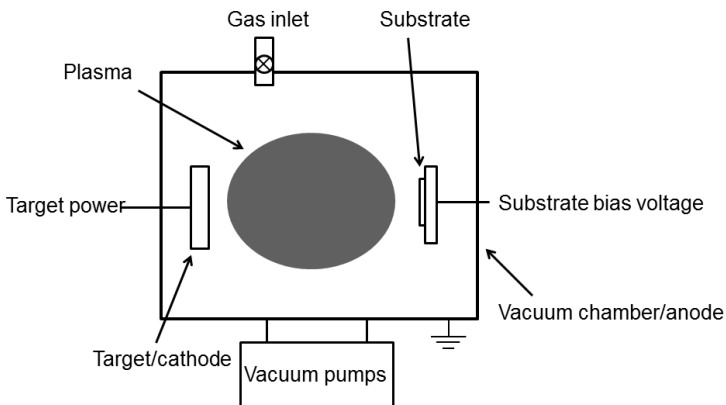


Figure 3.1: Schematic drawing of a sputtering system.

## 3.2 DC glow discharge

A plasma is a quasi-neutral gas of charged and neutral particles characterized by a collective behavior [36]. Quasi-neutrality means that there are equal amounts of ions and electrons, in addition to the neutral particles, and the overall charge is zero. The plasmas encountered in DC sputter deposition are typically formed at low pressures and have a low degree of ionization, typically  $10^{-4}$  [2]. For sputtering plasmas, the name glow discharge is often used because of the light emitted when atoms excited by collisions in the plasma lose their energy.

When a DC voltage, from a high-impedance power supply, is first applied to electrodes immersed in a low pressure gas, the low number of charge carriers present in the gas will yield a low current. If the voltage is increased, the charged particles will receive enough energy to create more carriers through impact with neutral gas atoms and ion collisions with the cathode, which release secondary electrons. The secondary electrons are accelerated away from the cathode by the electric field and ionize the working gas by inelastic collisions which result in the formation of a new ion-electron pair. The newly formed ions will be accelerated back towards to cathode and the formation of a new secondary electron is possible. This charge multiplication makes the current increase rapidly, while the voltage is constant due to the high impedance of the power supply. This is known as the Townsend discharge.

As the number of ejected secondary electrons further increases, these will eventually produce enough ions to regenerate the same number of initial electrons. When this happens, the discharge becomes self-sustainable and starts to glow, the voltage drops and the currents rises abruptly. This is known as the normal glow region. At first, the ion bombardment will be confined to surface irregularities and edges but by further increasing the power the bombardment will spread out and cover the entire cathode. If the power is further increased the result will be higher voltage and current densities. This region is called the abnormal discharge and it is in this domain sputter deposition is carried out.

Not every ion-cathode collision results in the emission of a secondary electron. Therefore, in order to sustain the plasma, the probability of collisions between the neutral gas atoms and the electrons has to be sufficiently high. If the pressure in the chamber is too low, the mean free path of the electrons will become long and the probability for collisions too low. The electrons will be lost to the chamber walls and the plasma will not be able to sustain itself. On the other hand, if the pressure is too high the frequent collisions will prevent the

electrons from gaining enough energy to ionize gas atoms and the discharge will be quenched. For a simple DC sputtering setup, an optimum pressure range typically of 0.1-10 Pa exists. In this range, the discharge can be sustained at reasonable voltages in the range 200-1000 V [37].

Because of their lower mass, the electrons in the discharge have a much higher mobility than the ions and will tend to reach the borders of the discharge at a much faster rate, compared to the ions. Any isolated surface immersed in the plasma will therefore start charging negatively. As the negative charge builds, additional electrons are repelled, positive ions are attracted, and the rate at which the surface is charging decreases. Ultimately, the electron flux will equal the ion flux and the net current will be zero. The surface will be at potential slightly negative with respect to ground, known as the floating potential. For the same reason, the plasma itself will be at a slightly positive potential, which is known as the plasma potential. If the immersed surface is negatively biased the negative bias replaces the floating potential. The voltage distribution in the DC glow discharge is shown in figure 3.2. Around each of the electrodes, regions with a net positive space charge develop. These regions are called the anode sheath and cathode sheath. The electric fields in the plasma are restricted to these sheath regions. As the cathode is at a negative potential in order to attract positive ions, almost the entire potential difference between the electrodes is confined to the cathode sheath. When the ions are accelerated through the cathode sheath they gain a maximum kinetic energy of  $e(V_p+V_0)$ , see fig. 3.2, before impact with the cathode.

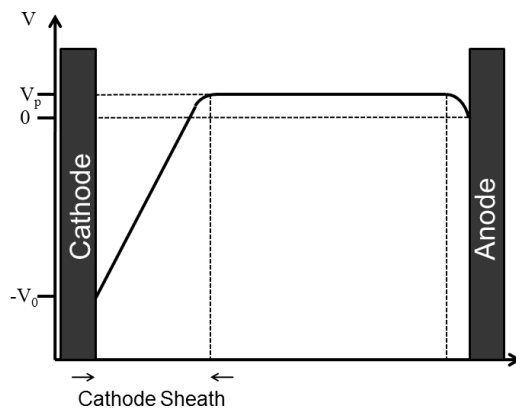


Figure 3.2: Schematic voltage distribution across a DC glow discharge.

### 3.3 The sputtering phenomenon

When the positive ions impact with the target, several interactions can occur. The ion can be implanted, recoil away from the target, or cause the important generation of secondary electrons. However, the intended process is the ejection of a target atom. Sputtering is the result of momentum transfer from the incoming ion to the target atoms through a collision cascade in the near surface region of the target. The average number of target atoms sputtered per incident ion is known as the sputtering yield,  $S$ .  $S$  depends on the mass of the incident ions and target atoms, the kinetic energy of incident ions, the heat of sublimation of an atom at the target surface, and the incidence angle of the ion [38].  $S$  can both be higher and lower than one depending on the material. In general, the sputtering yield of oxides is lower than the sputtering yield of pure metals due to their higher heat of sublimation.

### 3.4 Effects on the substrate

Compared to deposition by evaporation, sputtered atoms are more energetic when impinging on the substrate, and hence have higher adatom mobility. A way commonly used to influence the adatom mobility and film nucleation rate is the application of a substrate bias voltage which can result in altered film structure and properties [39]. By applying a negative bias voltage to the substrate, positive ions entering the sheath region at the substrate will be accelerated towards the growing film. In this way, the average energy of the particles arriving on the substrate surface can be substantially increased. The bombarding ions transfer energy and momentum to the atoms in the film surface and thereby provide atomic scale heating and higher adatom mobility. However, when high bias voltages are applied to the substrate resputtering can occur. In this case the substrate itself acts as a sputtering target and newly condensed species can be sputtered away. High bias voltages may also result in implantation of working gas ions in the growing film and/or increased defect formation in the crystal lattice. Applying positive bias voltage results in electron bombardment which is usually not useful for film modification. However, when depositing insulating films a pulsed bias voltage consisting of asymmetric positive and negative voltage polarities are applied. During the positive portion of the cycle, electrons are drawn to the film in order to neutralize the positive charge buildup that otherwise would cause arcs.

### 3.5 DC magnetron sputtering

Magnetron sputtering is one of the most widely used commercial techniques for thin film deposition. Compared to DC diode sputtering the use of a magnetron can significantly increase the deposition rate and reduce the operating pressure of the system.

The idea behind magnetron sputtering is to place permanent magnets behind the target in a suitable configuration in order to trap electrons near the target surface and thereby increase the degree of ionization as seen in figure 3.3. The electrons are subject to the Lorentz force

$$\mathbf{F} = m \frac{d\mathbf{v}}{dt} = e(\mathbf{E} + \mathbf{v} \times \mathbf{B}) \quad (3.1)$$

where  $m$  is the electron mass,  $e$  the electronic charge and  $\mathbf{v}$  is the electron velocity.  $\mathbf{B}$  and  $\mathbf{E}$  are the electric and magnetic fields, respectively. Electrons emitted at an angle slightly off the target normal will execute a helical motion along the magnetic fields emanating normal to the target. When reaching the region of the magnetic field parallel to the target the electrons are forced to move in an orbit back to the target. Solving the equations of motion, the electrons are found to move in cycloidal trajectories near the target.

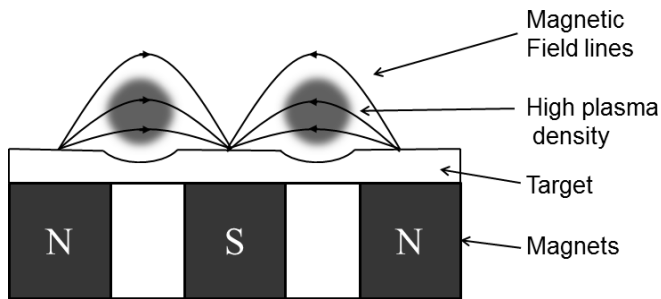


Figure 3.3: Schematic drawing of a magnetron configuration.

Generally, the magnetic field prolongs the residence time of the electron in the plasma, resulting in more collisions with the gas atoms, before being lost to the chamber walls. The result is an increased ionization of working gas atoms, leading to a higher

sputtering rate. By suitable orientation of the magnets, a region known as the race-track can be defined. In the race-track region the electrons hop around at high speed, efficiently ionizing the working gas. Therefore, sputtering is going on at the highest rate in this region, resulting in a characteristic erosion profile. This irregular erosion is one of the drawbacks of magnetron sputtering as only 20-30 % of the target material is utilized before the target has to be replaced.

### 3.6 Reactive sputtering

Reactive sputtering is the sputtering of an elemental or alloy target in the presence of a gas that reacts with the sputtered atoms and forms a compound. This is a useful technique that is widely applied for deposition of oxides, nitrides, and carbides. The reaction between the atoms and the reactive gas mainly occurs on surfaces as there is no mechanism which can dissipate the heat of the reaction to conserve both momentum and energy in a two-body system. This means that both the substrate and the target can be covered with a compound film. The reaction on the target is the source of a traditional problem in reactive sputtering. The sputtering yield of a compound is usually much lower than the sputtering yield of corresponding element. When the partial pressure of the reactive gas is so high that compound formation occurs faster than material can be sputtered away, the target gets covered with a compound film. It is then said to be *poisoned*. The resulting deposition rate will be low, but the films will be stoichiometric. If, on the other hand, the partial pressure is low or the sputter rate is high the atoms can be sputtered away from the target faster than a compound can be formed. The result is a high deposition rate but commonly understoichiometric films. This mode of deposition is called *metallic* mode. The transition from metallic to poisoned mode is often abrupt, and the increase in total pressure is often accompanied by significant changes in cathode voltage and current when operating in constant power mode. Furthermore, the reactive gas flow must be decreased well below the transition onset point to remove the compound formed on the target. This is a hysteresis effect. Often a partial pressure is chosen so the deposition takes place at the transition from a metallic target to a poisoned target, as this mode will result in stoichiometric films and a reasonable deposition rate. The transition region is, however, unstable and a feedback control of the partial pressure is required.

Today, the basic feedback signals commonly used to control the partial pressure are an optical emission spectrometer, an integrated mass spectrometer, a lambda sensor (for O<sub>2</sub> only), or the use of the cathode voltage as a feedback mechanism [40]. The latter can be used in a feedback loop as the shift from metallic to poisoned mode is associated with a drop in cathode voltage when running at constant power. The reason is a higher secondary electron emission coefficient for compound than the elemental/alloy target.

### 3.7 Pulsed DC magnetron sputtering

As mentioned above in the discussion of reactive sputtering, reactive gases often form dielectric coatings on metal-target surfaces. The positive ions bombarding the target cannot be neutralized by the electrons from the target because of the formation of an isolating film. When this happens, a positive charge starts to build-up on the surface, which may eventually become as large as the dielectric breakdown value of the compound layer. The result will be arcing, where much of the discharge current is concentrated on a small surface area of the target and a subsequent ejection of macro-particles from the target, leading to inhomogeneities and defects in the film [41].

Pulsation of the voltage supplied to the sputtering targets is the solution to prevent charging and arcing. The basic principle is that positive charging of the target can be avoided by discharging the surface by bombarding it with electrons. The voltage pulses can either be square or sinusoidal with applied frequencies of several kilohertz. Two common ways of discharging the target are switching the voltage to ground (unipolar) or switching to a slightly positive voltage (bipolar). The high mobility of the electrons is the reason for choosing only a slightly positive value, typically 10 % of the numerical value of the negative bias, to discharge in the bipolar mode. After discharging, the target is negatively powered and sputtering takes place.

### 3.8 Setup

The system employed to deposit all coatings presented in this work is a commercial CemeCon 800/9 SinOx coating unit with a chamber size of 850 x 850 x 1000 mm. It is able to cover substrates at a maximum size of 400 mm in diameter and 850 mm in height. The system is

equipped with two turbomolecular pumps (1900 l/s each) and a rotary vane type backing pump (18 l/s) to reach a base pressure below 1 mPa. The pressure is measured by use of a Pirani gauge. Ar (99.999%) and Kr (99.999%) are used as working gases while O<sub>2</sub> (99.999%) is supplied as a reactive gas for oxide formation. The flow rates of the gases are regulated by mass-flow-control units. During deposition, the O<sub>2</sub> partial pressure is controlled through a cathode current feedback mechanism to gain a stable deposition of the oxide thin film. When using this feedback mechanism, the hysteresis behavior of the system first needs to be determined at the conditions chosen for the deposition. During deposition, the system is operated a constant cathode voltage, known to result in deposition in the transition region when operating at a certain target power. A cathode current set-point is chosen to obtain the sought cathode power. Changes in the oxygen partial pressure result in changes in the cathode current away from the set-point due to compound formation or removal on the target surface. The feedback loop regulates the oxygen to bring the current back to the set-point.

Up to four targets can be mounted in the chamber, however only two are used when depositing YSZ (*paper 1*) or CGO (*papers 2 and 3*). The targets measure 88 × 500 mm<sup>2</sup> and are operated in unipolar mode (Advanced Energy, Pinnacle II supply) with a repetition frequency of 50 kHz and a duty cycle of 50 %. Substrates are mounted in the middle of the chamber and perform a 2-fold planetary rotational motion during deposition. Substrate bias voltage is applied as an asymmetric bipolar pulse (Advanced Energy, Pinnacle Plus supply) with a repetition frequency of 350 kHz and a positive pulse set to 10 % of the numerical value of the negative bias.

## 4. CHARACTERIZATION TECHNIQUES

---

In order to characterize the deposited thin films, several analysis techniques are used. The choice of analysis method depends on the properties one wishes to investigate, the resources available, the precision needed, and of the nature of the materials under investigation. In this section, a brief description of the characterization methods used in this thesis is given.

### 4.1 X-ray Diffraction (XRD)

XRD is applied for structural analysis of materials. It is a versatile technique which can be used for determining a number of microstructural properties of thin films, such as the crystalline phase, film orientation, epitaxial relations, grain size, and lattice strain [42,43]. Atoms in crystals are ordered in a three dimensional periodic structure within distinct volumes. As X-rays have wavelengths of the order of  $1 \text{ \AA}$ , which is comparable to the interatomic spacing in crystals, detection of discrete diffraction patterns is possible. When X-ray radiation interacts with matter, it can be elastically scattered. Scattering on periodic arrays of atoms in crystals results in constructive and destructive interference which gives rise to the diffraction pattern. This phenomenon can be described mathematically by Bragg's law

$$2d \sin \theta = n\lambda \quad (4.1)$$

where  $d$  is the lattice spacing,  $\theta$  the scattering angle,  $\lambda$  the wave length of the X-rays, and  $n$  is an integer number. During XRD measurements, a range of diffraction angles is scanned and the diffraction intensity is recorded as a function of angle. The resulting X-ray pattern or diffractogram can be viewed as a "fingerprint" of the crystal structure and used for identification of the material by comparing with diffraction standards from databases. Several examples of X-ray diffractograms can be seen in *paper 3* where the technique has been used to probe for SrZrO<sub>3</sub> formation in the samples.

The standard mode of operation is the  $\theta$ - $2\theta$  scan geometry. In this geometry, the angle of the incident beam and the detector are continuously varied, but they make equal angles with respect to the sample throughout the scan. Therefore, only planes parallel to the surface are probed. The recorded diffraction pattern is used for determining the crystal phase. For thin

films, it is often also interesting to determine the preferred orientation, or texture, of the sample. This is done by comparing the relative intensity of the peaks in the recorded spectrum to the relative intensities of the peaks in a randomly oriented reference sample from the database. Lattice strain is another interesting parameter which can be detected by observing small shifts in peak position due to changes in lattice distance. By analyzing the broadening (full width at half maximum) of the recorded peaks, one can draw conclusions on the grain size of the crystallites (coherence volumes) that makes up the sample as well as microstrain induced by the distortions in the crystal structure. In this work, XRD has primarily been used for determining crystal phases and preferential orientation, but changes in lattice strain and grain size has also been addressed in *paper 1*.

## 4.2 Scanning Electron Microscopy (SEM)

The SEM [44,45] is one of the most widely used instruments for coating characterization as it provides easily understood images of the sample and is simple to use. In the SEM, a beam of electrons, generated by a filament or field emission gun, is accelerated (at a voltage usually in the range of 3 - 20 keV), and focused by magnetic lenses onto a point on the sample which is scanned repeatedly. The interaction between the sample surface and the electron beam results in the emission of secondary electrons, backscattered electrons, and X-rays, all of which can be used to gather information about the specimen. The emitted electrons need to be detected and transformed into an electric current to form an image. Secondary electrons have the smallest sampling volume and are therefore capable of giving a better spatial resolution than backscattered electrons. The number of ejected secondary electrons depends on the orientation of the scanned surface with respect to the incident electron beam. A surface perpendicular to the incident beam emits fewer secondary electrons than a sloping surface. As a result, detection of secondary electrons gives a high topological contrast. The number of backscattered electrons emitted is proportional to the atomic number of the specimen atoms. Therefore, detection of backscattered electrons results in a compositional contrast. The SEM has a maximum resolution of a few nanometers, however the useful magnification of SEM images ranges from a few 100 times to several 100000 times depending on the features under investigation. In this work, SEM is used for imaging of sample surfaces and cross-sections in order to study film coverage of the substrate, surface topography, and morphology. By cross-

sections film thicknesses have been determined. Examples of micrographs can be found in all three included papers.

### 4.3 Transmission Electron Microscopy (TEM)

As implied by the name, TEM [46,47] is used to obtain structural information from samples thin enough to transmit electrons. Similar to SEM, a beam of electrons is generated by a filament or field emission gun, accelerated towards the sample, and focused by magnetic lenses onto a point on the sample. However, the energy of the electrons is in the order of 100 to 400 keV which is much higher than in SEM. The wavelength of electrons are given by the de Broglie relationship

$$\lambda = \frac{h}{\sqrt{2mqV}} \quad (4.2)$$

where  $h$  is Planck's constant,  $m$  the electron mass,  $q$  the electron charge, and  $V$  is the potential drop. The wavelength of the electrons is therefore in the range of picometers, but because of imperfect lenses the resolution of the TEM is limited to the order of 1 Å. This means atomic size resolution is possible with TEM. To achieve high quality data from the TEM, the sample needs to be thinned to approximately 50 nm in order to reduce multiple scattering when electrons transverse through the sample. This requirement makes sample preparation time-consuming and requiring skill.

When electrons pass through the sample they can be transmitted or scattered. By applying different objective apertures, different modes of imaging are possible. Bright-field images are obtained by intentionally excluding all diffracted beams and only allowing the central beam through the objective aperture. In this mode, contrast is formed by diffraction and mass thickness. Therefore crystalline areas and thicker samples will appear dark. Dark-field images can be formed by blocking out the central beam which gives the inverse contrast of bright field imaging. Instead of using an aperture for imaging, one can record the electron diffraction pattern. Selected area electron diffraction (SAED) makes it possible to probe only a desired area and obtain information about the crystal structure, lattice spacing, and orientation. Examples of TEM images and SAED patterns can found in *paper 1*. Here, SAED

is applied in order to study any epitaxial relationship between YSZ films grown on YSZ substrates while imaging has been used to study the microstructure of the films.

Scanning TEM is a mode of operation where the electron beam is condensed to a spot size of  $\sim 1$  nm and scanned across the sample, as in the SEM. The transmitted signal is then collected as a function of beam location, typically by a high-angle annular dark field (HAADF) detector. The contrast is mass and thickness dependent. It is possible to combine STEM mode with other techniques, typically energy dispersive x-ray spectroscopy (EDX) or electron energy loss spectroscopy. In this thesis, STEM has been combined with EDX to map the elemental concentrations in the samples as seen in *paper 3*.

#### 4.4 Energy Dispersive X-ray Spectroscopy (EDX or EDS)

EDX [48] is an analytical method for probing the chemical composition, often found integrated in SEM and TEM equipment. When the accelerated beam of electrons used for probing in SEM/TEM hits the sample, electrons from an inner shell of a sample atom may be ejected. An electron from an outer shell will fill the hole and emit X-rays in the process. As the energy of the X-ray depends on the electronic structure of the atom, identification and quantification of the elements in the sample is possible. EDX is best suited for quantification of “heavy” elements ( $Z > 10$ ). Quantification of light elements is less precise due to low X-ray yields and low energy of the X-rays. H, He, and Li cannot be detected. Therefore, this technique is well supplemented with other techniques for determination of chemical composition, such as Elastic Recoil Detection Analysis (ERDA), which is most sensitive for light elements. This has been done in *paper 1* for deposited YSZ thin films.

When performing EDX measurements, one can choose either to make a rapid determination of the elements present in the sample. Alternatively one can obtain information on the distribution of elements by performing a more time consuming mapping of the area of interest. STEM combined with EDX mapping was performed in *paper 3* in order to study Sr enrichment in CGO thin films due to diffusion.

## 4.5 Ion-beam analysis

Elastic Recoil Detection Analysis (ERDA) [49] is an ion-beam analysis technique used to determine the elemental composition of the thin films. In this technique, the sample is irradiated by a beam of heavy ions such as chlorine, iodine, or gold ions at energies of several MeV. In this work, a beam of 40 MeV  $^{127}\text{I}^{9+}$  has been used. The angle of incidence is lower than  $90^\circ$  resulting in target atoms being knocked out and recoiled in the forward direction. At the detector a mix of scattered projectiles and recoiled targets atoms will arrive with overlapping energies. By measuring the particle velocities in addition to the particle energies using a time-of-flight energy (ToF-E) detector, it is possible to resolve both for energy and mass and thereby distinguish the different particles. The information obtained by ERDA is a combination of mass, composition, and depth profiling. ERDA has a high sensitivity towards light elements such as C, O, and H but cannot distinguish between heavier elements with almost the same mass, such as Y and Zr which are neighbors in the periodic table. In this work, ToF-E ERDA has been used in *paper 1* to determine film composition in combination with EDX which is not accurate for light elements but can separate Zr from Y.

Rutherford Backscattering Spectrometry (RBS) is another ion-beam technique closely related to ERDA. In RBS, a high-energy ion beam with low-mass ions, typically  $\text{He}^+$ , is directed at the sample at a normal incidence angle, and the energies of the ions which are scattered backwards are analyzed. The energy of the backscattered atoms depends on the atomic mass of the target atoms and the depth at which the scattering event occurs. The information obtained by RBS is therefore a composition and depth profile of the sample. Like ERDA, RBS cannot distinguish between heavy element neighbors such as Y and Zr. Furthermore, detection of light elements is inaccurate due to the low backscattering yield.



## 5. CELL TESTING

---

In this section, a short introduction is given to the cell testing [50] performed in *paper 2* in order to assess the performance of fuel cells containing the deposited thin films.

No general agreement on test procedures exist which often makes it difficult to compare reported results. Therefore, a precise description of the applied test procedure must be given when presenting data. Extensive cell testing is usually only carried out on single cells or cell components. Full stack tests, which incorporate multiple cells and system components, are expensive and the results can be difficult to analyze. However, stack tests are conducted to assess the commercial viability of a setup.

In this work, fully assembled cells consisting of anode, electrolyte, and cathode have been tested in a single cell setup. A typical setup for testing of planar SOFCs is to place the cell in a test house sandwiched between gas distribution plates. The edges of the cell are effectively sealed in the test house by a glass seal to prevent gas leaking. On each side of the cell Pt or Au foils are placed to pick up the electrode current. The test house has built-in inlets and outlets for fuel and air as well current collectors, voltage probes, and thermocouples for measuring the temperature. The whole assembly is heated in a furnace to achieve the desired testing temperature before testing is started.

### 5.1 Polarization curves

The most common method used to characterize the performance of SOFCs is to examine current density-voltage polarization curves, as seen in figure 5.1, which yield information on the performance losses in the cell or stack under operating conditions. The performance of the cell can be determined in different ways, for example power density. However, the power output is highly dependent on fuel composition and cell voltage and can therefore be a diffuse measure. I-U curves for SOFCs are approximately linear, which allows the use of area-specific resistance (ASR) as an appropriate measure of performance. Largely the ASR value depends only on the temperature and is defined as

$$ASR = \frac{EMF - U}{i} \quad (5.1)$$

where  $EMF$  is the electromotive force, and  $U$  is the cell voltage at the current density,  $i$ , at the design point for the measurement. Measured ASR values are in general stated together with  $U$  value, fuel and air utilization, and operation temperature.

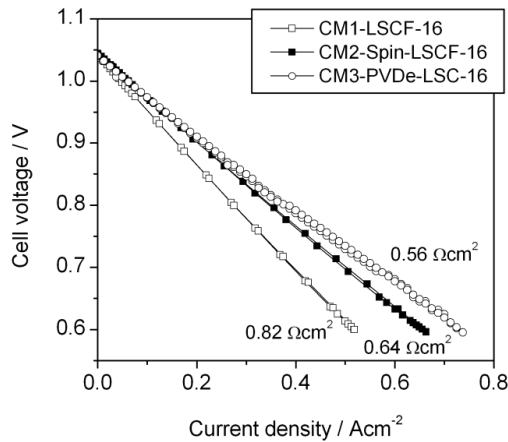


Figure 5.1: Polarization curves from cell testing of three different cells. ASR values are given next to the curves. Figure from *paper 2*.

## 5.2 Electrochemical Impedance spectroscopy (EIS)

EIS is a powerful technique for the characterization of electrochemical systems as it has the ability to distinguish between influences from different processes, such as reaction/migration steps [17,51]. The experimental procedure involves subjecting the cell to an AC signal of frequencies ranging from a few mHz to several hundred kHz and measuring the impedance response. Because each migration step or reaction, ideally, has a unique time constant associated with it, the distribution of the relaxation times enabled one to separate the different loss contributions in the cell.

Impedance spectra can be presented by plotting the negative imaginary part of the impedance as a function of real part (a Nyquist plot) or as a function of frequency (a Bode plot). Both representations are shown in figure 5.2. As the two representations depict different details, both are usually shown. In the Nyquist plot, a cell process is seen as a semicircle. In

fuel cells, where various processes occur the response will be a superposition of a number of semicircles. In contrast to the Nyquist plot, the Bode representation shows the frequency dependency. In this work, the Bode plot is combined with ADIS (analysis of differences in impedance spectra) spectra. ADIS is a way to visualize differences between two spectra by looking at the differences between the real part derivatives of the two Bode plots [52].

Impedance spectroscopy is used in *paper 2* to find responses that may explain differences in measured ASR values, such as SrZrO<sub>3</sub> formation in the cathode-electrolyte interface.

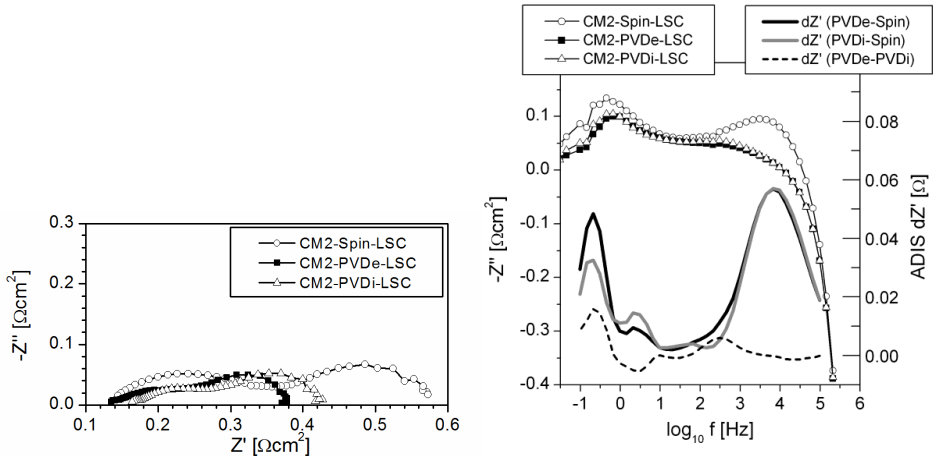


Figure 5.1: Left: Nyquist representation of impedance spectra from three different cells. Right: Combined Bode and ADIS representation of the impedance spectra. Figures from *paper 2*.



## 6. SUMMARY OF THE APPENDED PAPERS

---

### 7.1 Deposition of YSZ

Previous investigations have demonstrated laboratory scale deposition of YSZ thin films by magnetron sputtering [12,13,53-56]. For industrial applications, it is important to address the deposition time and throughput to keep the cost low enough to be competitive. At the same time, the quality of the deposited coatings needs to be reproducible and uniform throughout the coating area of the entire production unit. When up-scaling from laboratory scale to industrial scale, these requirements pose a challenge. This is particularly true when depositing oxides by reactive sputtering which is known to cause a hysteresis effect, non-uniformity of the films, and poor reproducibility [40].

In *Paper 1*, we address these challenges by depositing YSZ films in an industrial setup on both Si(001) and commercial NiO-YSZ SOFC anodes. The thin films were grown on both Si(001) and commercial tape cast NiO-YSZ anodes for fuel cell application and the texture, morphology, and composition of the deposited films were investigated. When depositing on Si(001) bias-dependent texturing of the resulting films was observed. These films were prone to form a columnar microstructure which is presumably unfavorable, as it may lead to leaks [55]. By increasing the substrate bias voltage columnar film growth could be prevented. Films deposited on NiO-YSZ substrates were columnar both at high and low bias voltage, however, the size of the columns were dependent on substrate bias. At high bias voltage, the columns were up to 10 times wider than observed at floating potential which resulted in a denser film that might be less permeable to gas. TEM investigations of films deposited on NiO-YSZ substrates showed that low bias (-30 V) caused randomly oriented films. At higher bias, a pronounced template effect was observed which resulted in films having the same orientation as the underlying substrate. Therefore, these films could not have any overall texture as the substrate consists of NiO and YSZ grains with random orientation. ERDA and EDX measurements of samples placed throughout the coating zone during depositions were used to show homogenous YSZ coatings could be deposited over large areas within the coating zone of the sputtering unit. This is important for industrial applications as the prospect of

producing uniform coatings across large surface areas is a requirement for the application of sputtered thin film electrolytes.

## 7.2 Deposition of CGO

In addition to the electrolyte, having an efficient cathode is highly important for the performance of the SOFC [57]. In order to apply novel cathodes, such as LSCF and LSC, a CGO barrier is needed between the cathode and the YSZ electrolyte. Earlier studies have shown that sputtering is an efficient way to produce CGO barrier coatings due to the high density of the sputtered films [15,25]. Previous studies have been carried out using the 2<sup>nd</sup> generation of ceramic SOFC. In *paper 2* we expand these studies by addressing deposition and testing of CGO barriers on metal-based cells.

This study focuses on comparing the electrochemical performance of cells containing sputter deposited or spin-coated CGO barriers, LSCF or LSC cathodes, and cermet backbones for the anode with different concentration of the ceramic Y-doped ZrO<sub>2</sub>. Testing was performed on cells with an active area of either 0.5 cm<sup>2</sup> or 4 cm<sup>2</sup>.

CGO coatings were deposited on the fuel cell electrolytes by reactive magnetron sputtering. Most fuel cell electrolytes were mounted directly on the substrate mounting platform. However, a few electrolytes were mounted electrically insulated from the mounting platform. This was done to reduce the ion bombardment during film growth. All other deposition parameters were kept constant. Comparing the microstructure, the sputtered films were found to be homogenous. Samples in direct electrical contact with the mounting station appeared to be slightly denser and less columnar. In contrast, the spin-coated barrier was both uneven in thickness, discontinuous, and porous. Cell testing showed that for cells with sputtered CGO barriers and LSC cathode, ASR values down to 0.27Ω cm<sup>2</sup> could be achieved at 650 °C. This is significantly better than standard ceramic cells with the LSM cathode as these cells have an ASR value in the range of 0.5 Ω cm<sup>2</sup> at 750 °C. Impedance data indicated that the less dense spin-coated CGO layer failed due Sr diffusion and SrZrO<sub>3</sub> formation.

To further improve sputtered CGO barriers, it is of great interest to understand the Sr diffusion mechanism in order to tailor the microstructure of the barrier layer in such a way that Sr diffusion may be prevented.

In *paper 3*, we study the diffusion mechanism of Sr and the formation of SrZrO<sub>3</sub>. Furthermore, we investigate the influence of film thickness and applied substrate bias voltage on the effectiveness of reactively sputtered CGO barrier coatings at different temperatures. To do so, a model system consisting of a base layer of sintered LSCF/CGO composite cathode material, a sputter deposited CGO barrier, and a thin top layer of YSZ was set up to simulate a fuel cell. This setup made it possible to follow Sr diffusion by observing the appearance of a SrZrO<sub>3</sub> peak by in-situ XRD.

It was found that 600 nm and 1.2 μm thick CGO barriers would break at 900 °C and 950 °C, respectively. TEM/EDX showed the diffusion to take place along grain/column boundaries. The observed elongated shape of the SrZrO<sub>3</sub> precipitates was attributed to a high driving force for SrZrO<sub>3</sub> formation and a limited Zr diffusion to the reaction zone. The SrZrO<sub>3</sub> only formed above LSCF grain in the LSCF-CGO composite and would not spread out sufficiently along the YSZ-CGO interface to form a fully covering layer, leaving patches open for conduction of ions. By depositing at higher substrate voltage denser films could be produced which were able to withstand higher temperatures before Sr diffusion was observed. This observation supports the finding of column boundaries as the major diffusion route.



## 7. CURRENT ACTIVITIES AND FUTURE PLANS

---

Based on the work presented so far, several studies can be performed and some has already been started. To narrow down the possibilities, I will focus on the following four issues.

### **Deposition of YSZ and CGO by High Power Impulse Magnetron Sputtering (HiPIMS)**

The work presented so far has focused on deposition of YSZ and CGO thin films by reactive pulsed DC magnetron sputtering. As seen in *paper 1* and *paper 2*, these thin films have been successfully deposited and, as also seen in *paper 2*, the presented CGO coating has a significant positive effect on the cell performance. However, as shown in the papers, it is difficult to prevent the deposited films from growing with a columnar morphology.

HiPIMS is an emerging technique for thin film deposition. Inherent to this technique is a high fraction of ionization of the sputtered material which favors the growth of dense films [58]. Therefore, it is of interest to deposit both YSZ and CGO by HiPIMS.

### **Further studies of CGO deposition**

Based on the promising results shown in *paper 2* additional work is being done on CGO deposited by pulsed DC magnetron sputtering. From the knowledge gained on Sr diffusion through CGO shown in *paper 3*, I hope to further increase the effectiveness of sputtered CGO as diffusion barriers.

In *paper 2*, we showed a well performing CGO barrier implemented in metal-based fuel cells. One goal is to develop a CGO barrier that will work on ceramic-based anode supported cells. This task has proved more difficult as the ceramic-based are sintered at higher temperatures. A second goal is to study deposition parameter variations, based on *paper 2* and *3*, in order to obtain better barrier performance and at the same time simplify and shorten the process to demonstrate the economic potential of the coating technique. Shortening the process time will increase throughput and lower unit production costs.

### **YSZ and CGO bilayer coatings**

*Paper 1* and *paper 2* deal with deposition of YSZ and CGO, respectively. It would be of interest to combine these results and deposit both the YSZ electrolyte and the CGO barrier by sputtering in a fuel cell setup.

### **Upscaling and stack testing**

To further test the developed CGO in setups that more closely resembles the planned end design of the SOFC stack I will utilize the capacity of the applied coating unit and coat cells for up-scaled cell tests. This includes testing of large cells (up  $12 \times 12 \text{ cm}^2$ ) in stack setups counting up to 50 cells.

## 8. REFERENCES

---

- [1] R. F. Bunshah, in : R. F. Bunshah (Eds.), *Handbook of Deposition Technologies for Films and Coatings*, 2<sup>nd</sup> ed., Noyes Publications, New Jersey, USA (1994), chapter 1.
- [2] W. R. Grove, *Philosophical Transactions of the Royal Society of London* 142 (1852) 87-101.
- [3] *2010 Survey of Energy Resource: Executive Summary*, World Energy Council, London, UK (2010).
- [4] R. M. Ormerod, *Chemical Society Reviews* 32 (2003) 17-28.
- [5] M.A. Laguna-Bercero, *Journal of Power sources* 203 (2012) 4-16.
- [6] W. R. Grove, *Philosophical Transactions of the Royal Society of London* 133 (1843) 91-112.
- [7] A. B. Stambouli, *Renewable and Sustainable Energy Reviews* 15 (2011) 4507-4520.
- [8] J. M. Andújar, F. Segura, *Renewable and Sustainable Energy Reviews* 13 (2009) 2309-2322.
- [9] I. Kosacki, C. M. Rouleau, P. F. Becher, J. Bentley, D. H. Lowndes, *Solid State Ionics* 176 (2005) 1319-1326.
- [10] J. H. Shim, C.-C. Chao, H. Huang, F. B. Prinz, *Chemistry of Materials* 19 (2007) 3850-3854.
- [11] A. Karthikeyan, C.-L. Chang, S. Ramanathan, *Applied Physics Letters* 89 (2006) 183116.
- [12] F. Smeacetto, M. Salvo, L. C. Ajitdoss, S. Perero, T. Moskalewicz, S. Boldrini, L. Doubova, M. Ferraris *Materials Letters* 64 (2010) 2450-2453.
- [13] M. Sillassen, P. Eklund, M. Sridharan, N. Pryds, N. Bonanos, J. Bøttiger, *Journal of Applied Physics* 105 (2009) 104907.
- [14] C. Brahim, A. Ringuedé, E. Gourba, M. Cassir, A. Billard, P. Briois, *Journal of Power Sources* 156 (2006) 45-49.
- [15] F. C. Fonseca, S. Uhlenbruck, R. Nédélec, D. Sebold, H. P. Buchkremer, *Journal of The Electrochemical Society*, 157 (2010) B1515-B1519.
- [16] EG&G Technical Services Inc., *Fuel Cell Handbook*, 7<sup>th</sup> ed., National Energy Technology Laboratory, Morgantown, USA (2004).

- [17] S. C. Singhal, K. Kendall (Eds.), *High Temperature Solid Oxide Fuel Cells: Fundamentals, Design and Applications*, Elsevier Advanced Technology, Oxford, UK (2003).
- [18] J.-J. Choi, D-S. Park, B.-G. Seong, H.-Y. Bae, *International Journal of Hydrogen Energy* 37 (2012) 9809-9815.
- [19] L.R. Pederson, P. Singh, X.-D. Zhou, *Vacuum* 80 (2006) 1066-1083.
- [20] L. Blum, W. A. Meulenberg, H. Nabelek, and R. Steinberger-Wilckens, *International Journal of Applied Ceramic Technology* 2 (2005) 482-492.
- [21] J. H. J. S. Thijssen, *The Impact of Scale-Up and Production Volume on SOFC Manufacturing Cost*, National Energy Technology Laboratory, Morgan Town, USA (2007).
- [22] W. Z. Zhu, S. C. Deevi, *Materials Science and Engineering A* 362 (2003) 228-239.
- [23] C. Sun, R. Hui, J. Roller, *Journal of Solid State Electrochemistry* 14 (2010) 1125-1144.
- [24] P. Plonczak, M. Joost, J. Hjelm, M. Søggaard, M. Lundberg, P.V. Hendriksen, *Journal of Power Sources* 196 (2011) 1156-1162.
- [25] S. Uhlenbruck, N. Jordan, D. Sebold, H. P. Buchkremer, V.A.C Haanappel, D. Stöver, *Thin Solid Films* 515 (2007) 4053-4060.
- [26] R. Knibbe, J. Hjelm, M. Menon, N. Pryds, M. Søggaard, H. J. Wang, K. Neufeld, *Journal of the American Ceramic Society* 93 (2010) 2877-2883.
- [27] A.B. Stambouli, E. Traversa, *Renewable and Sustainable Energy Reviews* 6 (2002) 433-455.
- [28] S. J. Litzelman, J.L. Hertz, W. Jung, H. L. Tuller, *Fuel Cells* 0 (2008) 1-9.
- [29] M. C. Tucker, *Journal of Power Sources* 195 (2010) 4570-4582.
- [30] B. H. C Steele, *Solid State Ionics* 129 (2000) 95-110.
- [31] T. Van Gestel, D. Sebold, H. P. Buchkremer, D. Stöver, *Journal of the European Ceramic Society* 32 (2012) 9-26.
- [32] F. Han, R. Mücke, T. Van Gestel, A. Leonide, N. H. Menzler, H. P. Buchkremer, D. Stöver, *Journal of Power Sources* 218 (2012) 157-162.
- [33] B. C. H. Steele, A. Heinzl, *Nature* 414 (2001) 345-352.
- [34] J. Wu and X. Liu, *Journal of Materials Science and Technology* 26 (2010) 293-305.
- [35] M. K. Mahapatra, K. Lu, *Materials Science and Engineering R* 67 (2010) 65–85.
- [36] J. L. Vossen, W. Kern, *Thin Film Processes II*, Academic Press Inc., San Diego, USA (1991).

- [37] M. Ohring, *The Materials Science of Thin Films*, 2<sup>nd</sup> ed., Academic Press Inc., San Diego, USA (2002), chapter 4.
- [38] P. Sigmund, *Physical Review* 184 (1969) 383-416.
- [39] I. Petrov, P. B. Barna, L. Hultman, and J. E. Greene, *Journal of Vacuum Science and Technology A* 21 (2003) 117-128.
- [40] W. D. Sproul, D. J. Christie, D. C. Carter, *Thin Solid Films* 491(2005) 1-17.
- [41] P.J. Kelly, R.D. Arnell, *Vacuum* 56 (2000) 159-172.
- [42] D. Brandon and W. D. Kaplan, *Microstructural Characterization of Materials*, 2<sup>nd</sup> ed., John Wiley & Sons Ltd, West Sussex, England (2008), pp. 55-78.
- [43] M. Birkholz, *Thin Film Analysis by X-ray Scattering*, Wiley-VHC Verlag GmbH & Co. KGaA, Weinheim, Germany (2006).
- [44] M. Ohring, *The Materials Science of Thin Films*, 2<sup>nd</sup> ed., Academic Press Inc., San Diego, USA (2002), pp. 584-587.
- [45] P. J. Goodhew, F. J. Humphreys, R. Beanland, *Electron microscopy and analysis*, 3<sup>rd</sup> ed., Taylor & Francis (2001), pp.122-129.
- [46] D. Brandon and W. D. Kaplan, *Microstructural Characterization of Materials*, 2<sup>nd</sup> ed., John Wiley Sons Ltd, West Sussex, England (2008), pp. 179-235.
- [47] D. B. William and C. B. Carter, *Transmission Electron Microscopy: A Textbook for Materials Science*, Plenum Press, New York, USA (1996).
- [48] J. Goldstein, D. Newbury, D. Joy, C. Lyman, P. Echlin, E. Lifshin, L. Sawyer, and J. Michael, *Scanning Electron Microscopy and X-ray Microanalysis*, 3<sup>rd</sup> ed., Springer, New York, USA (2003), Chapter 9 and 10.
- [49] O. Benka, in: G. Friedbacher, H. Bubert (Eds.), *Surface and Thin Film Analysis; A Compendium of Principles, Instrumentation, and Applications*, 2<sup>nd</sup> ed., Wiley-VCH Verlag GmbH & Co. KGaA, Weinheim, Germany (2011), pp. 217-227.
- [50] M. Mogensen, P. V. Hendriksen in: S. C. Singhal, K. Kendall (Eds.), *High Temperature Solid Oxide Fuel Cells: Fundamentals, Design and Applications*, Elsevier Advanced Technology, Oxford, UK (2003), chapter 10.
- [51] E. Barsoukov, J. R. Macdonald (Eds.), *Impedance Spectroscopy: Theory, Experiment, and Applications*, 2<sup>nd</sup> ed., John Wiley & Sons, Inc., Hoboken, USA (2005).
- [52] S. H. Jensen, A. Hauch, P. V. Hendriksen, M. Mogensen, N. Bonanos, T. Jacobsen, *Journal of The Electrochemical Society* 154 (2007) B1325-B1330.
- [53] P. Briois, A. Billard, *Surface & Coatings Technology* 201 (2006) 1328-1334.

[54] P. Coddet, M.C. Pera, A. Billard, *Surface & Coatings Technology* 205 (2011) 3987-3991.

[55] S. Rey-Mermet, Y. Yan, C. Sandu, G. Deng, P. Mural, *Thin Solid Films* 518 (2010) 4743-4746.

[56] R. Nédélec, S. Uhlenbruck, D. Sebold, V.A.C. Haanappel, H.-P. Buchkremer, D. Stöver, *Journal of Power Sources* 205 (2012) 157-163.

[57] R. Barfod, A. Hagen, S. Ramousse, P. V. Hendriksen, M. Mogensen, *Fuel Cells* 6 (2006) 141-145.

[58] K. Sarakinos, J. Alami, S. Konstantinidis, *Surface & Coatings Technology* 204 (2010) 1661-1684.